



Synthesis and characterization of *N*-hydroxyphthalimide immobilized on SiO₂-coated Fe₃O₄ nanoparticles as magnetic catalyst for oxidation of benzyl alcohols and hydrocarbons

Rahman Hosseinzadeh¹ · Mohammad Mavvaji¹ · Mahmood Tajbakhsh¹ · Zahra Lasemi²

Received: 30 June 2017 / Accepted: 28 December 2017
© Iranian Chemical Society 2018

Abstract

In this study, *N*-hydroxyphthalimide (NHPI) was successfully attached on functionalized SiO₂-coated Fe₃O₄ nanoparticles through amid bond. The sustained nanomagnetite-immobilized NHPI as a new magnetically recoverable catalyst was characterized by FT-IR, XRD, TGA, VSM, TEM and SEM techniques. The prepared catalyst exhibited high selectivity for oxidation of various benzyl alcohols and hydrocarbons in the presence of hydrogen peroxide as oxidant. The catalyst can be readily separated from the reaction mixture using an external magnet and reused several times without significant loss of its catalytic activity.

Keywords *N*-hydroxyphthalimide · Nanomagnetic catalyst · Oxidation · Hydrogen peroxide · Benzyl alcohols · Hydrocarbons

Introduction

The development of facile and efficient systems for selective oxidation of organic substrates under mild and eco-friendly conditions is one of the most attractive and challenging issues in organic chemistry [1, 2]. In conventional methods, a stoichiometric amount of classical oxidants such as manganese dioxide [3], chromic acid [4] and hypervalent iodine [5] was utilized for the conversion of organic compounds into corresponding oxidized products. However, they are hazardous oxidizing agents, due to the formation of large amount of toxic wastes, along with harsh workup procedures. To overcome these problems, the catalytic oxidation process has been introduced as a promising improvement in this protocol. During two recent decades, a useful and feasible catalytic approach has been organized on the basis of using *N*-hydroxy imides (NHIs), and especially *N*-hydroxyphthalimide (NHPI), which have broadly

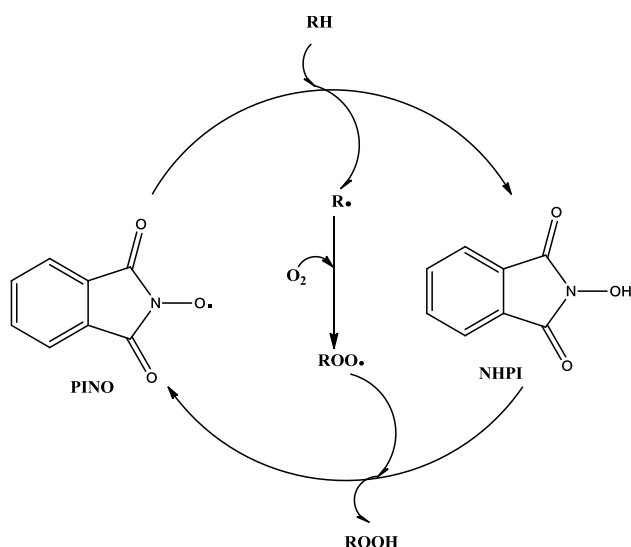
applied as desirable catalysts for the oxidation of organic substrates [6, 7]. *N*-hydroxyphthalimide has been considered as a valuable and powerful catalyst for the efficient oxidation of a wide range of organic compounds mainly alcohols [8] and alkyl aromatics [9]. Due to its non-toxic feature, simple preparation from phthalic anhydride and hydroxyl amine and high activity towards different types of organic substrates, this organocatalyst has attracted great attention in recent years. Theoretically, NHPI can proceed oxidation process via the initial production of phthalimide *N*-oxyl (PINO) radical, which subsequently abstracts hydrogen from substrate as illustrated in Scheme 1 [10]. Under oxidation conditions, these radicals effectively react with oxygen leading to form oxygen-containing products.

Generally, transition metal salts—mostly Co(II) [11], Cu(II) [12] and Mn(IV) [13] salts—have been employed as co-catalyst to accelerate generation of PINO radical. Despite effectiveness of these metal-based complexes, from the both economic and green chemistry aspects, they are not desirable. Hence, within the last decade, metal-free catalysis has been remarkably evolved and significant attempts have been accomplished in order to develop these systems in oxidation reactions. For example, Xu et al. have reported *o*-phenanthroline- [14] as well as, 1,4-diamino-2,3-dichloro-anthraquinone [15]-based metal-free catalytic system for the oxidation of various hydrocarbons.

✉ Rahman Hosseinzadeh
r.hosseinzadeh@umz.ac.ir

¹ Department of Organic Chemistry, Faculty of Chemistry, University of Mazandaran, Babolsar, Iran

² Department of Chemistry, Firoozkooh Branch, Islamic Azad University, Firoozkooh, Iran



Scheme 1 Mechanism of hydrocarbon oxidation in the presence of NHPI

On the other hand, the concept of heterogeneous catalyst is of great importance in the design of a chemical process owing to its recovery and reusability properties [16–18]. Therefore, the application of heterogeneous catalysts in liquid-phase oxidation has attracted growing interest due to simple separation from reaction media. Additionally, from the viewpoint of environmental concerns, decreasing the losses of either catalyst or solvent upon separation process causes avoiding unfavourable waste. In this regard, several reports have been focused on immobilization of NHPI into ionic liquids [19, 20] or onto solid support surfaces and polymers [21–24]. The recent works by Orlinska et al. showed that *N*-hydroxyphthalimide supported on functionalized polystyrene or poly (2-hydroxyethylacrylate-co-divinylbenzene) is capable of oxidizing toluene and *p*-methoxy toluene [25, 26].

In addition, Fe_3O_4 magnetic nanoparticles (MNPs) have been widely studied as simply accessible inorganic support with high surface area [27, 28]. On account of facile and quick separation and recovery, heterogeneous catalysts based on surface functionalized Fe_3O_4 nanoparticles have been found numerous applications in different fields and several report have been published about their catalytic performance in the oxidation of organic materials [29–31].

Accordingly, in continuation of efforts about extending metal-free catalytic oxidation and inspired by attempts accomplished by Xu and his co-workers, herein we report the immobilization of NHPI onto functionalized SiO_2 -coated Fe_3O_4 nanoparticles as a core-shell nanoparticle which successfully was employed for the oxidation of a series of benzyl alcohols, as well as hydrocarbons. It is notable that there is no any report about preparation of such magnetically

recoverable nanocatalyst for the oxidation of benzyl alcohols and hydrocarbons.

Experimental

Chemicals and materials

Tetraethylorthosilicate (TEOS, purity $\geq 99\%$), 3-(aminopropyl)-triethoxysilane (APTES, purity $\geq 97\%$), iron oxide nanopowder (Fe_3O_4 , purity $\geq 97\%$), trimellitic anhydride chloride (purity $\geq 98\%$) and ammonium hydroxide (NH_4OH , 28%) were purchased from Sigma-Aldrich and used without further purification. Other chemicals and also solvents were purchased from Merck Company and used as received.

Instrumentation

The X-ray powder diffraction (XRD) of the catalyst was performed on a Philips PW 1830 X-ray diffractometer with $\text{CuK}\alpha$ source ($\lambda = 1.5418 \text{ \AA}$) in a range of Bragg's angle (10° – 80°) at room temperature. Scanning electron microscope (SEM) analyses were taken using LEO

Scanning electron microscope (SEM) analyses were taken using LEO-1455VP microscope (acceleration voltage 10 kV). Transmission electron microscopy (TEM) experiments were conducted on a Zeiss-EM10C electron microscope with acceleration voltage 80 kV. Thermogravimetric analysis (TGA) was carried out on a Stanton Red craft STA-780 (London, UK). Analysis of magnetic properties was performed employing vibration sample magnetometer (VSM, MDK, and Model 7400) at room temperature. IR spectra were recorded on a FT-IR Bruker vector 22 spectrophotometer. Products of oxidation reactions were characterized using an Agilent Technologies 7890A/5975C gas chromatography (GC) with HP-5 MS capillary column.

Preparation of catalyst

Preparation of silica-coated magnetic nanoparticles ($\text{Fe}_3\text{O}_4/\text{SiO}_2$, SCMNPs) and 3-aminopropyl-modified SCMNPs (ASCMNPs)

Modification of the MNPs with a silica coating ($\text{Fe}_3\text{O}_4@ \text{SiO}_2$ core-shell structure) was performed as reported in the literature [32]. An amount of 1.0 g of the Fe_3O_4 was dispersed in 35 ml ethanol and 6 ml deionized water and then sonicated for 15 min. Afterwards, tetraethyl orthosilicate (TEOS) (1.5 ml) was added to the mixture and sonicated again for 10 min. After sonication, aqueous ammonia (28%, 1.4 ml) was added slowly and the reaction was allowed to proceed at 80°C for 12 h under continuous

magnetic stirring. The sustained silica-coated magnetic nanoparticles (SCMNPs) was separated from the solution by use of a permanent magnet and washed several times with distilled water and methanol, being dried at 25 °C under vacuum. For the next step, the prepared SCMNPs (2.0 g) were suspended in toluene (100 ml) via sonication and then 3-aminopropyl triethoxysilane (2.0 ml) was added to reaction mixture under argon atmosphere. The reaction progressed under reflux condition for 12 h. Then, the final attained solid was readily separated by external magnet and after washing with ethanol and acetone was dried under vacuum at 80 °C.

Preparation of silica-coated magnetic nanoparticle-supported NHPI

Obtained ASCMNPs (2.0 g) was suspended in 30 ml of CH_2Cl_2 with sonication, and then, trimellitic anhydride chloride (TAC) was added. After addition of triethylamine (Et_3N) dropwise over 1 h via syringe, the reaction mixture was allowed to stir for 24 h at room temperature and the resulting anhydride was magnetically separated, washed with ethanol and CH_2Cl_2 and dried under vacuum. The resulting product was added to 30 ml pyridine along with addition of hydroxylamine hydrochloride (0.2 g), and after that, the reaction mixture was stirred for 16 h at 90 °C. The product was magnetically separated, washed several times with methanol, ethanol and distilled water and finally was dried in an oven at 80 °C. The immobilized NHPI was characterized with FT-IR spectroscopy, X-ray diffraction, scanning and transmission electron microscopies and vibrating sample magnetometry.

Catalytic oxidation of benzyl alcohols and hydrocarbons in the presence of silica-coated magnetic nanoparticle-supported NHPI

Oxidation of benzyl alcohols and hydrocarbons was carried out in a 50-ml round-bottomed flask equipped with a condenser and a mechanical stirrer. Hydrogen peroxide (aqueous solution 30% (w/w) of H_2O_2) was used as oxidant. In a typical procedure, to a mixture acetonitrile (5.0 ml) solution of benzyl alcohol (1 mmol) was added catalyst (10 mg), *o*-phenanthroline (2.5 mol%), Br_2 (3 mol%) and the H_2O_2 (2 mmol). Then, the reaction mixture was heated at reflux temperature. After completion of the reaction, the catalyst was magnetically separated and the products were analysed using GC-MS measurements. Additionally, under the same reaction conditions, reactivity of tetralin and indane was examined and excellent conversion with high selectivity was observed.

Results and discussion

Preparation and characterization of the nanocatalyst

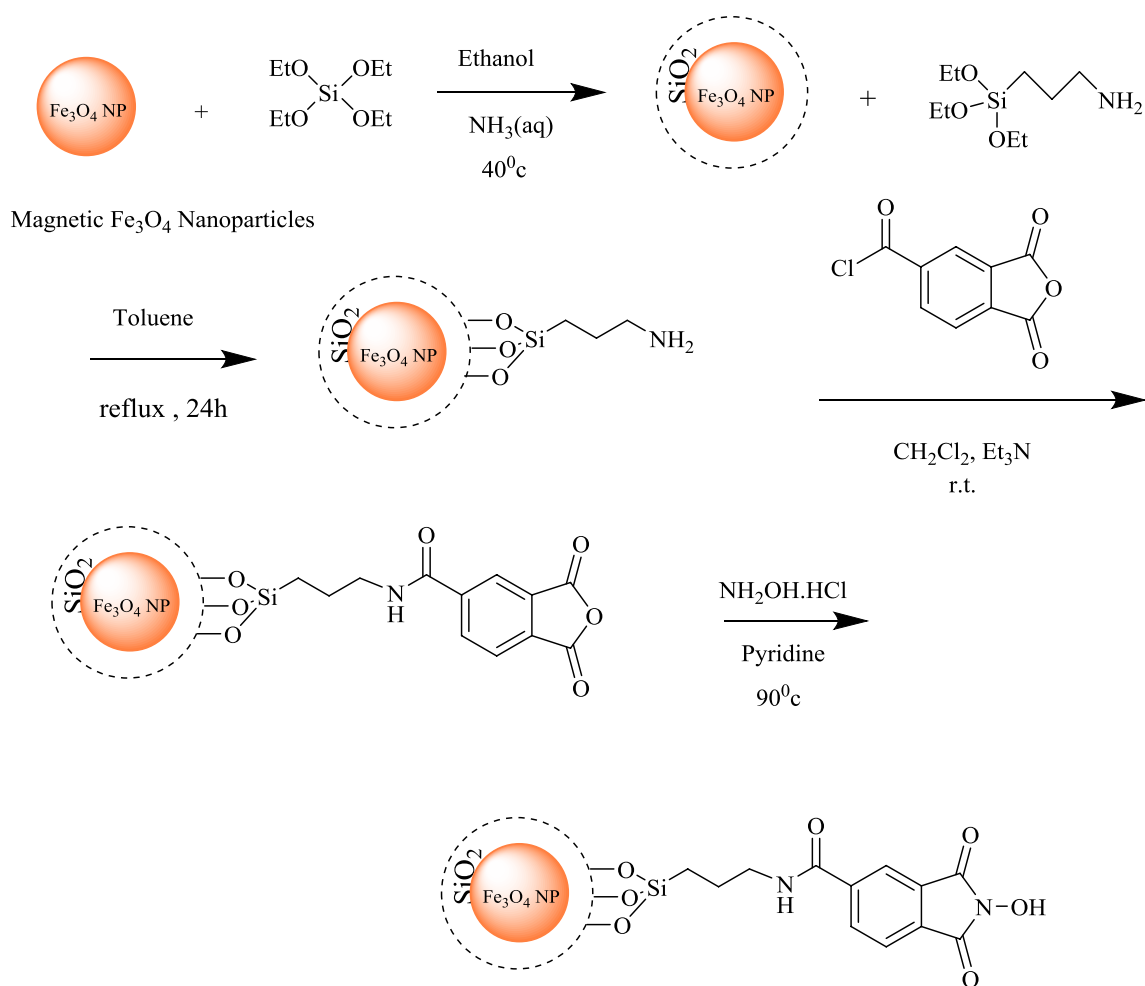
In this research, NHPI was successfully immobilized on silica-coated magnetite nanoparticles including aminopropyl groups via amide bonds. NHPI was appended on modified magnetic support as illustrated in Scheme 2. At first, silica-coated nanomagnetite (Nano $\text{Fe}_3\text{O}_4@\text{SiO}_2$) was prepared from Fe_3O_4 and tetraethoxysilane (TEOS) in the presence of ammonium hydroxide solution 28%. After that, this core-shell nanoparticle system was modified with 3-aminopropyl triethoxysilane (APTES). Then, the interaction between trimellitic anhydride chloride (TAC) and amino-functionalized SiO_2 —through amide bond—lead to the formation of immobilized TAC product. Eventually, this nanoparticle successfully converted to the final catalyst using hydroxylamine hydrochloride and pyridine.

Fourier transform infrared (FT-IR) analysis

FT-IR measurements were carried out in order to confirm the presence of characteristic peaks of prepared compounds, as shown in Fig. 1. Strong bands at 636 and 581 cm^{-1} , as well as, an absorption band at around 462 cm^{-1} (Fig. 1a) pertain to the Fe–O bond of magnetite. Furthermore, the drastic Si–O–Si stretching vibrations at the range of 1000–1100 cm^{-1} obviously represent the silica shell around Fe_3O_4 . The FT-IR spectrum of ASCMNPs (Fig. 1b) exhibited several signals in the area of 1450–1550 and 2850–2925 cm^{-1} , attributed to C–H stretching vibrations which arise from the presence of the propyl group. Moreover, two broad signals at 3445 and 1629 cm^{-1} are related to N–H group. In the FT-IR analysis of immobilized TAC (Fig. 1c) appeared new peaks at 1852 and 1777 cm^{-1} —relevant to carbonyl groups of anhydride. Additionally, absorption band emerged at 1632 cm^{-1} , evidently indicates the formation of amide bond between TAC moiety and ASCMNPs. As displayed in Fig. 1d, FT-IR spectrum of the final NHPI-based catalyst unveiled the disappearance of representative signal of anhydride group at 1852 cm^{-1} , along with shifting the frequencies of carbonyl bond at 1777 cm^{-1} (related to $\text{O}=\text{C}(\text{O})$) to 1785 cm^{-1} (ascribed to $\text{O}=\text{C}(\text{N})$) in which these results are in accordance with the formation of corresponding product. Nevertheless, distinguishing of *N*-hydroxyl group peak was difficult owing to overlapping with N–H stretching vibration at 3445 cm^{-1} .

X-ray diffraction (XRD) analysis

In order to investigate the crystalline structure of obtained products, X-ray diffraction (XRD) technique was utilized. As depicted in Fig. 2, all the samples displayed characteristic



Scheme 2 Synthesis of magnetic nanoparticle-supported NHPI using a $\text{Fe}_3\text{O}_4/\text{SiO}_2/\text{APTES}$ core-shell nanoparticle system as a nanomagnetic catalyst

peaks at 2θ values: 30.3, 35.6, 43.1, 53.8, 57.5 and 62.4 which correspond to the diffractions of (220), (311), (400), (422), (511) and (440), respectively. The relative intensities of diffraction peaks are properly in consistent with the standard XRD data related to Fe_3O_4 crystals with a spinel structure (JCPDS-19-0-0629). Moreover, according to XRD results shown in Fig. 2d, a negligible decline in the intensity along with broadening of the peaks was observed which may be ascribed to the decreasing of the scattering contrast between the Fe_3O_4 @ SiO_2 surface and the organic moiety immobilized onto it. Besides, these XRD patterns clearly reveal that immobilization process of NHPI-based moiety onto the surface of SiO_2 -coated nanomagnetite did not effect on the crystalline structure of Fe_3O_4 core.

Thermogravimetric analysis (TGA)

Evaluation of thermal stability and the amount of attached organic moiety on the surface of SiO_2 -coated nanomagnetite were carried out by thermogravimetric analysis (TGA) and derivative thermogravimetric (DTG) curve at the range of 20–800 °C. As shown in Fig. 3a, in the TGA curve of ASCMNPs observed a mass loss of about 1% in the range of 20–180 °C, ascribed to moisture and absorbed water, as well as, an overall weight loss of ~ 9% in the thermal region of 180–500 °C which arises from the decomposition of aminopropyl constituent. According to these results, the amount of APTES anchored on the SiO_2 -coated surface is calculated by use of the following Eq. (1):

$$\begin{aligned} \text{mmol of APTES} &= (\text{weight loss}/100 \times \text{Mw hydrolyzed APTES}) \times 1000 \\ &= (9.39/58 \times 100) \times 1000 = 1.62 \text{ mmol} \end{aligned} \quad (1)$$

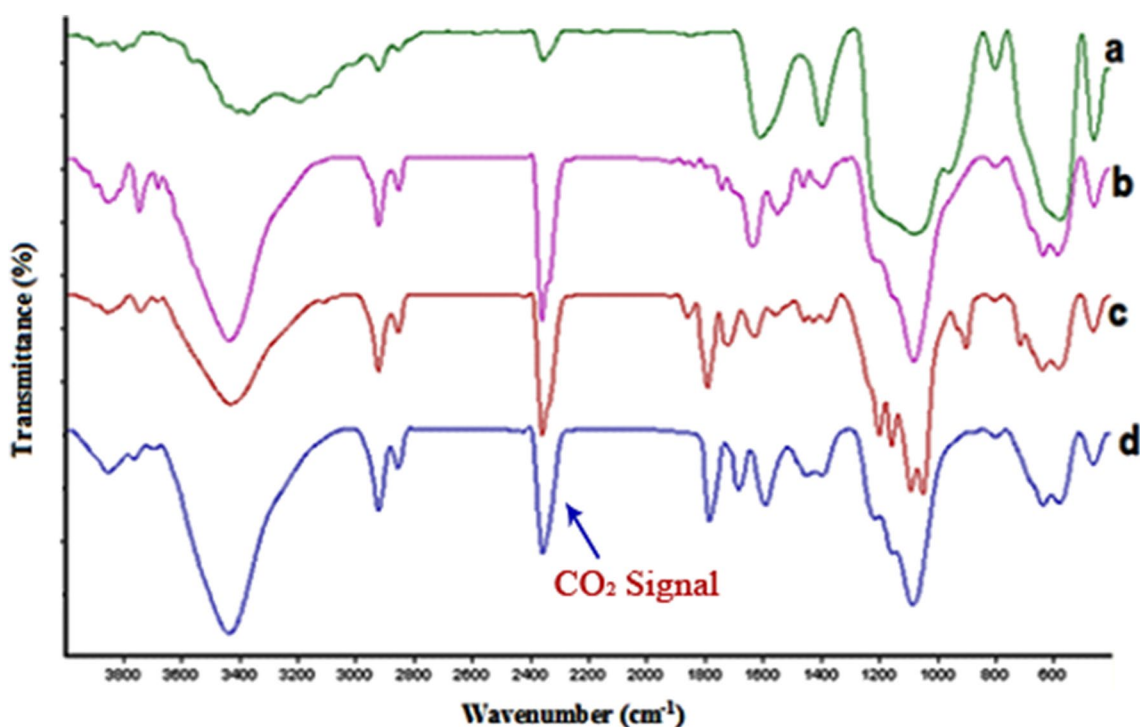


Fig. 1 FT-IR spectra for a SCMNPs, b ASCMNPs, c Fe_3O_4 @TAC and d Fe_3O_4 @NHPI catalyst

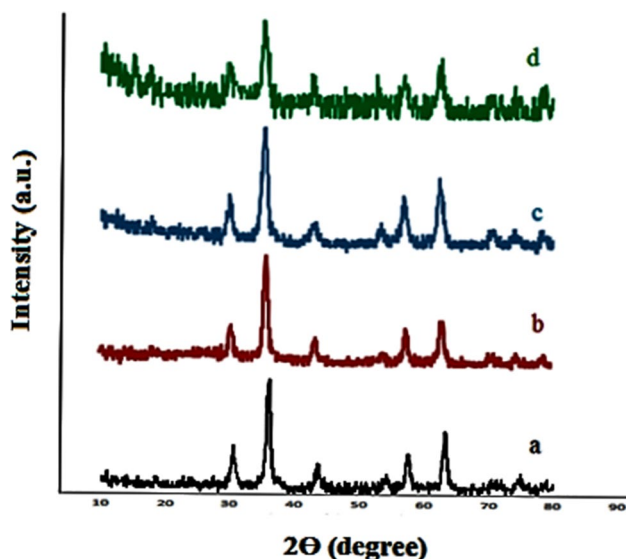


Fig. 2 XRD powder pattern of samples: a Fe_3O_4 @ SiO_2 , b ASCMNPs, c Fe_3O_4 @TAC and d Fe_3O_4 @NHPI catalyst

The TGA spectrum of MNPs@ TAC exhibited about 7% weight loss up to 180 °C, corresponding to water content of the sample, and the other mass change of ~ 37% which can be attributed to the release of TAC moiety immobilized on the MNPs@ SiO_2 core-shell system. Similar to ASCMNPs,

the amount of loaded TAC-amidopropyl is afforded by Eq. (2):

$$\begin{aligned} & \text{mmol of TAC-Amidopropyl} \\ &= (\text{weight loss}/100 \times \text{Mw TAC-Amidopropyl}) \times 1000 \\ &= (37/232 \times 100) \times 1000 = 1.59 \text{ mmol} \quad (2) \end{aligned}$$

Eventually, investigating the TGA and DTA curves of MNPs@ NHPI displayed a weight loss about ~ 2% in the temperature range of 20–180 °C, followed by a weight decrease of 29% related to separation of NHPI-based species grafted on MNPs surface in the area of 200–550 °C. Applying the calculative method mentioned above, the amount of NHPI-containing residue is attained by Eq. (3):

$$\begin{aligned} & \text{mmol of NHPI-Amidopropyl} \\ &= (\text{weight loss}/100 \times \text{Mw NHPI-Amidopropyl}) \times 1000 \\ &= (29/247 \times 100) \times 1000 = 1.17 \text{ mmol} \quad (3) \end{aligned}$$

VSM analysis

Analysis of magnetic properties of functionalized magnetite nanoparticles was performed using vibrating sample magnetometry (VSM). Considering the magnetization curves, present in Fig. 4, the magnetization saturation values for MNPs@ APTES, MNPs@ TAC and MNPs@ NHPI were obtained as 36.79, 28.9 and 17.34 emu g^{-1} ,

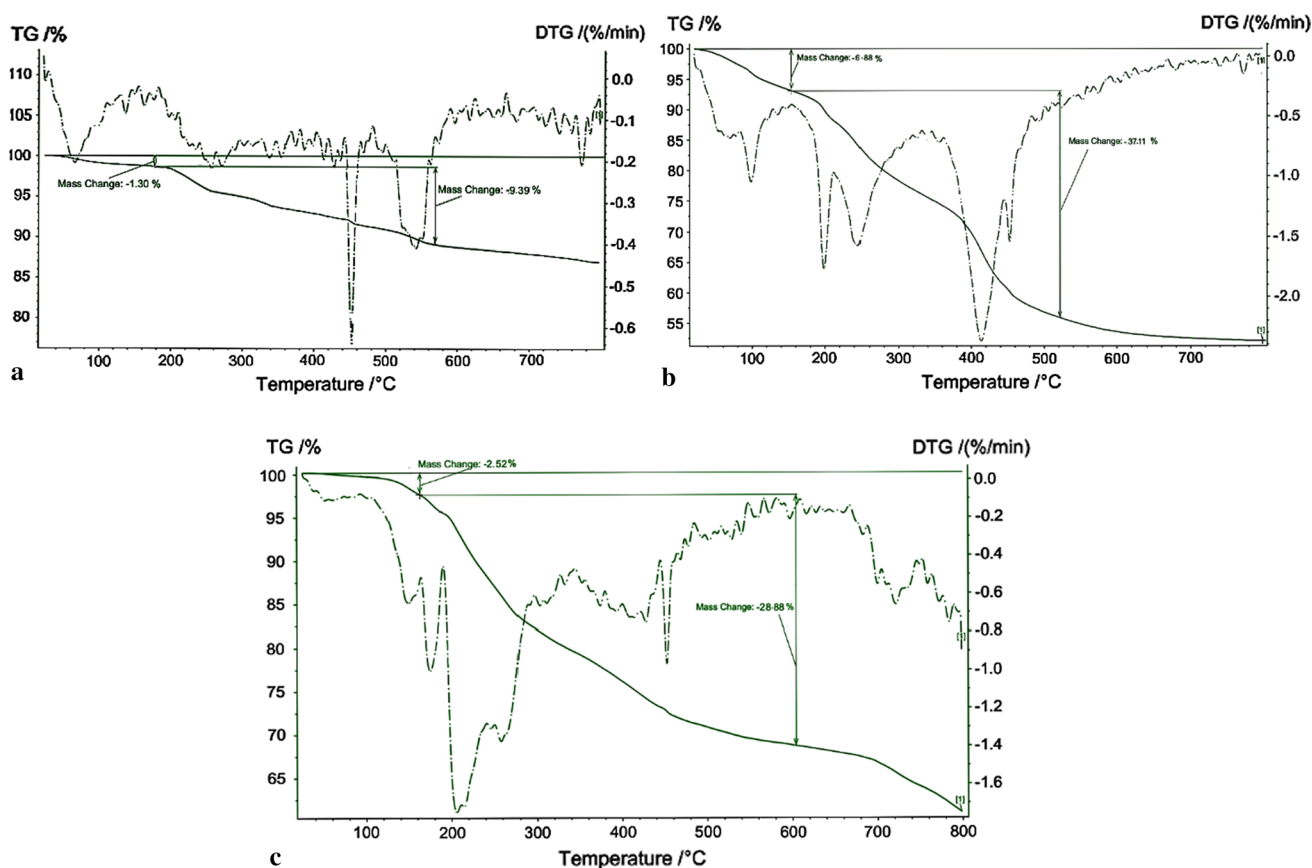


Fig. 3 The TGA/DTG curves of **a** MNP-coated APTES, **b** MNPs@TAC and **c** MNPs@NHPI

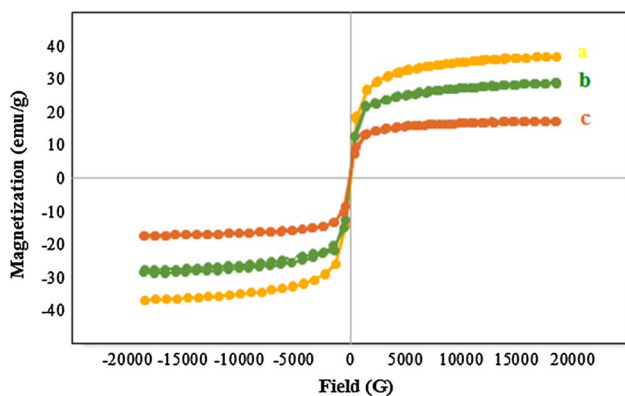


Fig. 4 Magnetization curves obtained by VSM at room temperature for **a** ASCMNPs, **b** Fe_3O_4 @TAC and **c** Fe_3O_4 @NHPI

respectively. According to these results, we observe a decreasing trend in magnetization characteristic along with increasing the amount of organic material loaded on MNPs@ SiO_2 surface which leads to extend non-magnetic part of product. Nonetheless, the synthesized MNPs@ NHPI readily separate from reaction medium in

the presence of an external magnetic field (supermagnet) and can be utilized as an efficient magnetically recoverable nanocatalyst.

Scanning electron microscopy (SEM)

Studying morphology of the Fe_3O_4 @ SiO_2 —before and after immobilization process—was accomplished using scanning electron microscope (SEM). As displayed in Fig. 5, the SEM micrographs of Fe_3O_4 @ SiO_2 and ASCMNPs exhibited a smooth surface with almost spherical shape. However, growth in particle size and agglomeration seem to be occurred after immobilization, owing to appendage of organic fragment on the surface of Fe_3O_4 @ SiO_2 - NH_2 nanoparticles.

Transmission electron microscopy (TEM)

To identify the morphology and particle size of prepared nanoparticles, transmission electron microscopy (TEM) analysis can be applied. As shown in Fig. 6, TEM images of ASCMNPs (a) and MNPs@ NHPI (b) demonstrate their

Fig. 5 The SEM images of **a** $\text{Fe}_3\text{O}_4@\text{SiO}_2$, **b** ASCMNPs, **c** $\text{Fe}_3\text{O}_4@\text{TAC}$ and **d** $\text{Fe}_3\text{O}_4@\text{NHPI}$

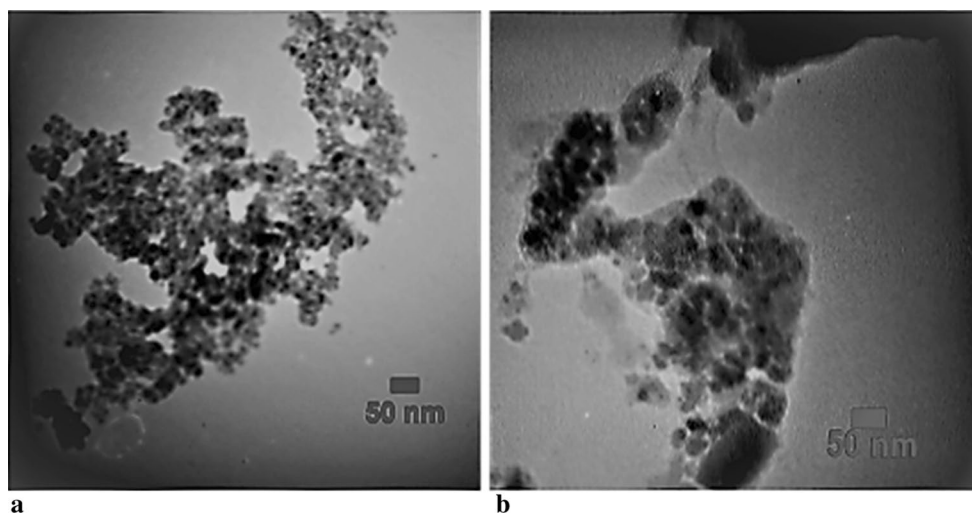
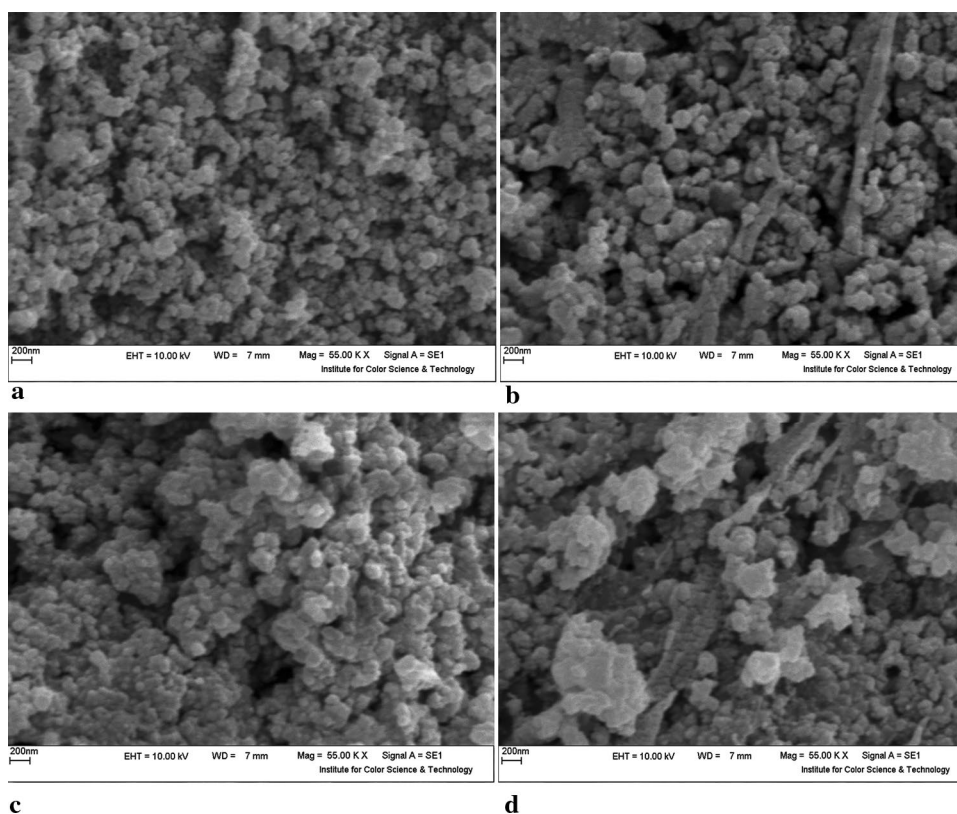
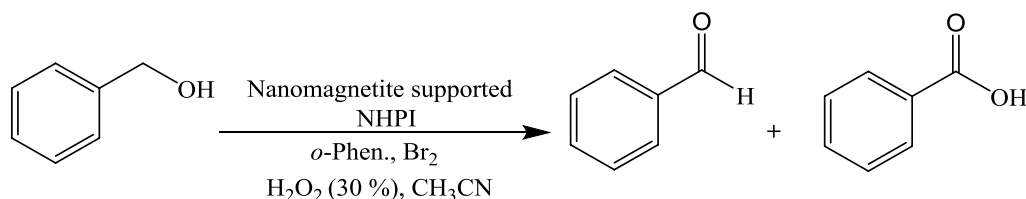


Fig. 6 The TEM images of **a** ASCMNPs, and **b** $\text{Fe}_3\text{O}_4@\text{NHPI}$ nanoparticles

nearly spherical shape with obtained particle size of 15 and 19 nm, respectively. Comparison of these values indicates grafting the NHPI-containing segment onto the $\text{Fe}_3\text{O}_4@\text{SiO}_2$ modified with APTES which resulted in size enlargement.

Catalytic application of $\text{Fe}_3\text{O}_4@\text{NHPI}$ nanoparticles

The catalytic efficiency of synthesized nanomagnetite-immobilized NHPI was examined in oxidation reaction of benzyl alcohols and hydrocarbons. For this purpose, oxidation reaction of benzyl alcohol was chosen as a model

Table 1 Reaction conditions screening for oxidation of benzyl alcohol

Entry	Amount of catalyst (mg)	H ₂ O ₂ 30% (mmol)	Temperature (°C)	Time (h)	Conversion (%) ^a	Selectivity (%) ^b
1	10	1.5	25	4	35	83
2	10	1.5	50	4	50	88
3	10	1.5	80	4	81	95
4	5	1.5	80	4	65	82
5	20	1.5	80	4	83	90
6	10	1	80	6	70	78
7	10	2	80	3	85	97
8	10	2.5	80	3	86	91

^aAmounts of conversion and selectivity were measured by GC–MS analysis

^bSelectivity towards the benzaldehyde

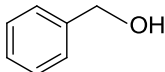
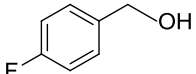
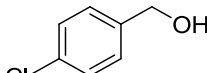
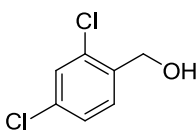
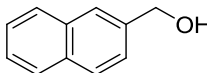
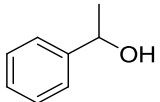
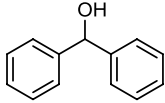
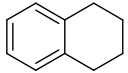
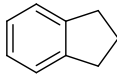
reaction in which the results are summarized in Table 1. When benzyl alcohol (1 mmol) was reacted with aqueous solution of H₂O₂ (30% (w/w), 1.5 mmol) in the presence of nanomagnetite-immobilized NHPI (10 mg), *o*-phenanthroline (2.5 mol%) and Br₂ (3 mol%) in acetonitrile at different temperatures (25, 50, 80 °C), benzaldehyde was obtained with high selectivity (95%) within 4 h (Table 1, entries 1–3). During the course of further optimization of the reaction conditions, model reaction was carried out in different amount of catalyst (nanomagnetite-immobilized NHPI). According to these results, 10 mg of catalyst was sufficient to promote the oxidation process (Table 1, entries 3–5). Additionally, the reaction resulted in low yield of product in the absence of catalyst. The influence of amount of H₂O₂ (30% aqueous solution as oxidant) was also examined. The above experiment was performed in different quantities of H₂O₂ (Table 1, entries 3 and 6–8). The best amount of H₂O₂ (30%) was found in 2 mmol, which gave benzaldehyde with 97% selectivity after 3 h. Further increasing the amount of H₂O₂ (30%) did not improve the degree of conversion and selectivity (Table 1, entry 8).

Then, the sustained optimal conditions were applied to oxidize various organic compounds (Table 2). As present in Table 2, various benzyl alcohols derivatives were impressively converted to the corresponding carbonyl products with high selectivity. Benzyl alcohol converted to benzaldehyde with 97% selectivity. Benzyl alcohols including electron-withdrawing groups on phenyl ring such as 4-fluoro and 4-chloro benzyl alcohol (Table 2, entries 2–3) showed 95 and 86% conversion with 90%

and 80% selectivity for corresponding benzaldehyde, respectively, along with the low quantities of 4-fluoro and 4-chloro benzoic acid. Similarly, 2,4-dichloro benzyl alcohol (Table 2, entry 4) exhibited 76% conversion and 79% selectivity towards 2, 4-dichloro benzaldehyde. On the other hand, 2-naphthalenemethanol (Table 2, entry 5) displayed the lowest reaction time with considerable amounts of conversion and selectivity (conversion 91% and selectivity 92%). Secondary benzyl alcohols also were examined under optimum reaction conditions (Table 2, entries 6 and 7). As shown in Table 2, 1-phenylethanol and diphenyl methanol were oxidized exclusively to acetophenone and benzophenone, respectively. However, despite the high degree of conversion and selectivity for most of benzyl alcohol derivatives, reaction of furfuryl alcohol did not lead to related 2-furfural and in this case, mainly afforded levulinic acid and 4-hydroxycyclopent-2-one, instead. Furthermore, hydrocarbons also effectively reacted under these conditions. Tetralin and indane remarkably converted to 1-tetralone and 1-indanone, respectively, in conjunction with low amounts of 1-tetralol and 1-indanol (Table 2, entries 8–9).

One of the most important parameters in exploring performance efficiency of heterogeneous catalyst is recoverability and reusability which can evidently describe the stability of catalyst during the catalytic process. To survey the reusability and recovery properties of the catalyst, it was separated after completion of the reaction and was utilized for next run of our model reaction under the same condition. By virtue of magnetic character of nanocatalyst, it was readily

Table 2 Oxidation of various substrates through Fe₃O₄@NHPI-based catalysed system^a

Entry	Starting material	Time (h)	Conversion ^b (%)	Selectivity (%) ^{b,c}
1		3	85	97
2		4.5	86	80
3		3.5	95	90
4		4.15	76	79
5		1.5	91	92
6		2.5	98	–
7		2.5	100	–
8		1.45	93	94
9		2	91	92

^aReaction conditions: catalyst (10 mg), starting material (1 mmol), *o*-phen (2.5 mol%), Br₂ (3 mol%) oxidant (2 mmol) in 5 mL CH₃CN at 80 °C

^bInformation about the conversion of starting materials and selectivity of corresponding products were obtained by GC–MS analysis

^cSelectivity towards the benzaldehyde and ketone derivatives

separated by employing an external magnet, as displayed in Fig. 7, and was washed several times with ethanol.

After being dried in an oven at 70 °C, it was ready to be utilized for next reaction. According to our experimental results, this nanomagnetic catalyst could be successfully

recovered and reused up to four times without considerable loss of activity in comparison with fresh catalyst (Fig. 8). The stability and recyclability of the catalyst predominantly originate from the SiO₂ shell around nano-Fe₃O₄ which protect it against oxidation throughout the cycle. It is noteworthy that the TEM and IR analysis of recovered catalyst (Figs. 9 and 10) did not showed any remarkable change after using four times.

Based on plausible mechanism suggested by Xu et al. [14], a mechanistic pathway has been elucidated for the catalytic oxidation process. Initially, *o*-phenanthroline—as co-catalyst—is converted to a cation-radical species in the presence of Br₂. Then, the proton and electron transfer between this cation-radical and NHPI-containing catalyst resulted in formation of PINO radicals (Scheme 3). After that, the generated PINO intermediate abstracts hydrogen from substrate (benzyl alcohol or hydrocarbon) and turns it into radical. The resulting radical could possibly react with oxygen generated in situ from decomposition of hydrogen peroxide in the presence of Br₂ [33, 34] leading to the corresponding peroxy radicals. Finally, these radicals abstract hydrogen atom from NHPI to generate PINO radical and hydroperoxide which undergoes an elimination process to provide the desired product as shown in Scheme 1.

Conclusions

In this work, immobilization of NHPI on functionalized silica-coated magnetite nanoparticles through amide bond has been successfully accomplished. This novel-synthesized magnetic heterogeneous catalyst was well characterized by FT-IR, XRD, TGA, TEM, VSM and SEM techniques. The prepared compound exhibited considerable activity in oxidation reactions of benzyl alcohols and hydrocarbons. The starting materials were selectively converted to corresponding carbonyl-containing products with high yields. Moreover, one of the most advantageous features of this type of heterogeneous catalysts is facile and fast separation and recovery procedure via an external magnet. Based on empirical results, the recovered catalyst was reusable for next runs up to four times with no impressive change in its catalytic effect.

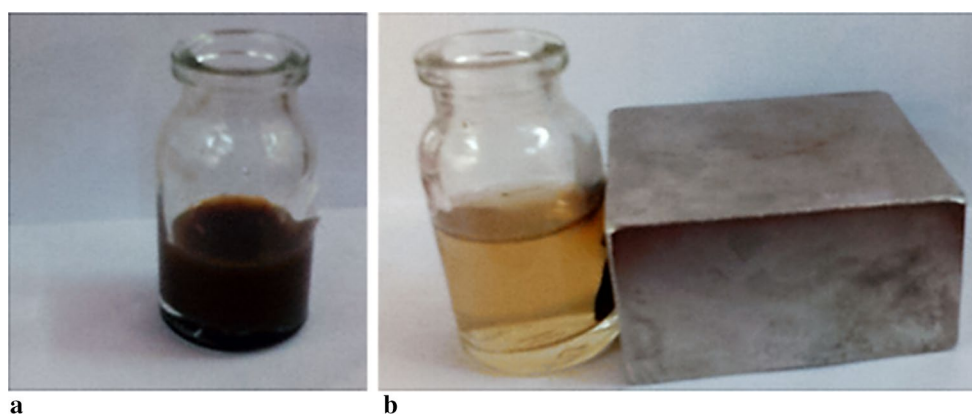


Fig. 7 Reaction mixture of benzyl alcohol **a** before, and **b** after magnetic separation

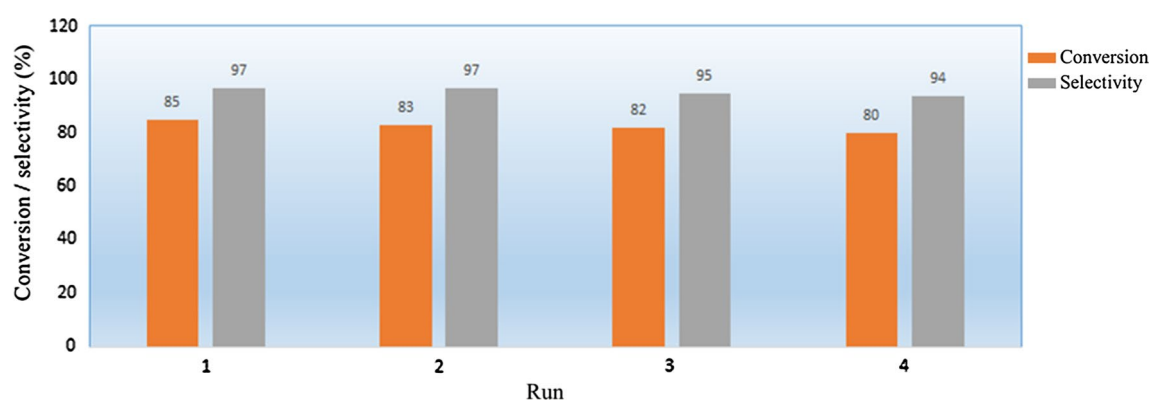


Fig. 8 Reusability study of $\text{Fe}_3\text{O}_4@\text{NHPI}$ for oxidation of benzyl alcohol under optimized conditions

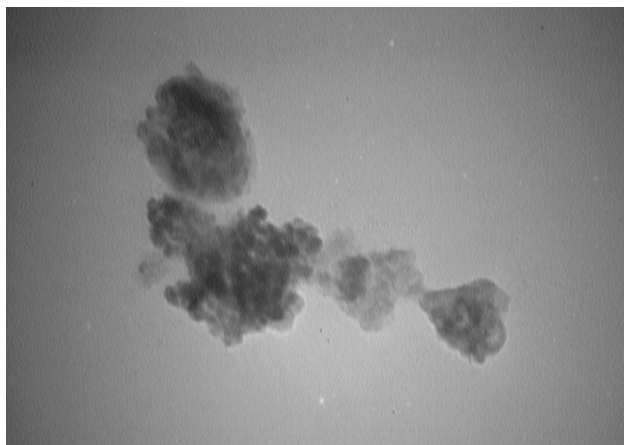
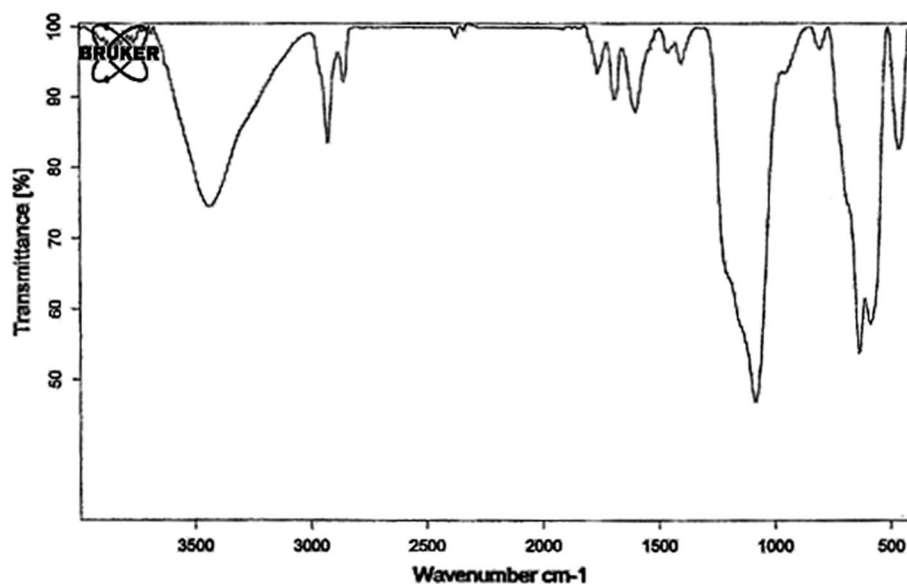
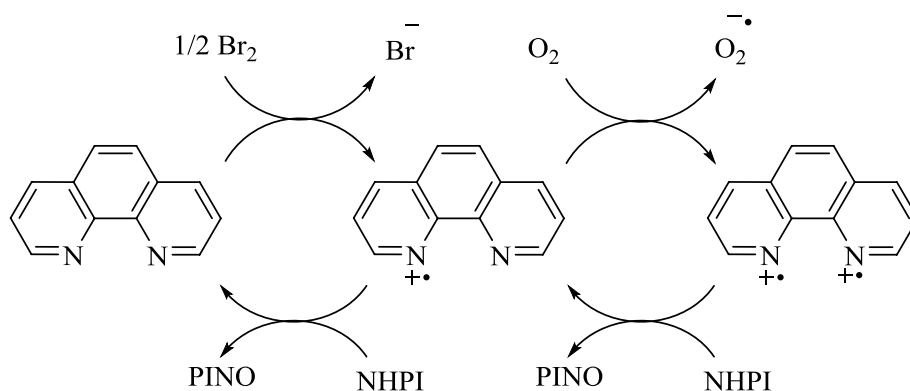


Fig. 9 The TEM image of reused $\text{Fe}_3\text{O}_4@\text{NHPI}$

Fig. 10 FT-IR spectra of reused $\text{Fe}_3\text{O}_4/\text{NHPI}$



Scheme 3 PINO radical generation



Acknowledgement Financial support of this work from the Research Council of the University of Mazandaran is gratefully acknowledged.

References

- J.E. Bäckvall, *Modern Oxidation Methods* (Wiley-VCH Verlag GmbH & Co. KGaA, Weinheim, Germany, 2012)
- T. Mallat, A. Baiker, *Chem. Rev.* **104**, 3037 (2004)
- M. Hudlicky, *Oxidations in Organic Chemistry* (American Chemical Society, Washington, 1990)
- S.V. Ley, A. Madfin, *Comprehensive organic synthesis* (Pergamon, Oxford, 1991)
- H.G. Aurich, K. Hahn, K. Stork, W. Weiss, *Tetrahedron* **33**, 969 (1977)
- F. Recupero, C. Punta, *Chem. Rev.* **107**, 3800 (2007)
- C. Galli, P. Gentili, O. Lanzalunga, *Angew. Chem. Int. Ed.* **47**, 4790 (2008)
- S. Coseri, *Mini-Rev. Org. Chem.* **5**, 222 (2008)
- S. Coseri, *Catal. Rev. Sci. Eng.* **51**, 218 (2009)
- R. Amorati, M. Lucarini, V. Mugnaini, G.F. Pedulli, F. Minisci, F. Recupero, F. Fontana, P. Astolf, L. Greci, *J. Org. Chem.* **68**, 1747 (2003)
- B.B. Wentzel, M.P.J. Donners, M.C. Feiters, P.L. Alsters, R.J.M. Nolte, *Tetrahedron* **56**, 7797 (2000)
- B. Orlin'ska, *Tetrahedron Lett.* **51**, 4100 (2010)
- J. Jiang, Y. Jing, Y. Zhang, N. Zhang, J. Jiao, W. Zhu, H. Xue, Y. Zong, G. Yang, *Catal. Lett.* **141**, 544 (2011)
- X. Tong, J. Xu, H. Miao, *Adv. Synth. Catal.* **347**, 1953 (2005)
- G. Yang, Y. Ma, J. Xu, *J. Am. Chem. Soc.* **126**, 10542 (2004)
- M.G. Clerici, O.A. Kholdeeva, *Liquid Phase Oxidation via Heterogeneous Catalysis: Organic Synthesis and Industrial Applications* (John Wiley & Sons, Hoboken, 2013)
- M. Arshadi, M. Ghiaci, *Appl. Catal. A* **399**, 75 (2011)
- G. Huang, A.P. Wang, S.Y. Liu, Y.A. Guo, H. Zhou, S.K. Zhao, *Catal. Lett.* **114**, 174 (2007)
- S. Koguchi, T. Kitazume, *Tetrahedron Lett.* **47**, 2797 (2006)
- J.R. Wang, L. Liu, Y.F. Wang, Y. Zhang, W. Deng, Q.X. Guo, *Tetrahedron Lett.* **46**, 4647 (2005)
- F. Rajabi, J.H. Clark, B. Karimi, D.J. Macquarrie, *Org. Biomol. Chem.* **3**, 725 (2005)
- I. Hermans, J. Van Deun, K. Houthoofd, J. Peeters, P.A. Jacobs, *J. Catal.* **251**, 204 (2007)
- M. Jian, C. Jianlan, L. Dongmei, X. Meina, *RSC Adv.* **6**, 68170 (2016)
- S. Su, J.R. Giguere, S.E. Schaus, J.A. Porco, *Tetrahedron* **60**, 8645 (2004)
- K. Kasperczyk, B. Orlinska, E. Witek, P. Łatka, J. Zawadiak, L. Proniewicz, *Catal. Lett.* **145**, 1856 (2015)

26. P. Łątka, K. Kasperczyk, B. Orlińska, M. Drozdek, B. Skorupska, E. Witek, *Catal. Lett.* **146**, 1991 (2016)
27. C.O. Dalaigh, S.A. Corr, Y. Gunko, S.J. Connon, *Angew. Chem. Int. Ed.* **46**, 4329 (2007)
28. A.H. Latham, M.E. Williams, *Acc. Chem. Res.* **41**, 411 (2008)
29. L. Chen, B. Li, D. Liu, *Catal. Lett.* **144**, 1053 (2014)
30. P.S. Rathore, R. Patidarb, S. Thakore, *RSC Adv.* **4**, 41111 (2014)
31. M.V. Kirillova, C.I.M. Santos, W. Wu, Y. Tang, A.M. Kirillov, *J. Mol. Catal. A: Chem.* **426**, 343 (2017)
32. J. Wang, S. Zheng, Y. Shao, J. Liu, Z. Xu, D. Zhu, *J. Colloid Interface Sci.* **349**, 293 (2010)
33. W.C. Bray, R.S. Livingston, *J. Am. Chem. Soc.* **50**, 1654 (1928)
34. J.H. Baxendale, *Adv. Catal.* **4**, 31 (1952)